MATERIALS SCIENCE

Realizing a 14% single-leg thermoelectric efficiency in GeTe alloys

Zhonglin Bu, Xinyue Zhang, Bing Shan, Jing Tang, Hongxia Liu, Zhiwei Chen, Siqi Lin, Wen Li, Yanzhong Pei*

GeTe alloys have recently attracted wide attention as efficient thermoelectrics. In this work, a single-leg thermoelectric device with a conversion efficiency as high as 14% under a temperature gradient of 440 K was fabricated on the basis of GeTe-Cu_2Te-PbSe alloys, which show a peak thermoelectric figure of merit (zT) > 2.5 and an average zT of 1.8 within working temperatures. The high performance of the material is electronically attributed to the carrier concentration optimization and thermally due to the strengthened phonon scattering, the effects of which all originate from the defects in the alloys. A design of Ag/SnTe/GeTe contact successfully enables both a prevention of chemical diffusion and an interfacial contact resistivity of 8 microhm·cm^2 for the realization of highly efficient devices with a good service stability/durability. Not only the material's high performance but also the device's high efficiency demonstrated the extraordinariness of GeTe alloys for efficient thermoelectric waste-heat recovery.

INTRODUCTION

Thermoelectric technology enables a direct conversion between heat and electricity for both refrigeration and power generation applications. A high thermoelectric conversion efficiency requires a large temperature difference between the hot and cold sides ($\Delta T = T_h - T_c$) and a high materials' dimensionless figure of merit, defined as $zT = (S^2T)/\rho(\kappa_E + \kappa_L)$, where S, T, ρ, κ_E, and κ_L are Seebeck coefficient, absolute temperature, resistivity, and electronic and lattice components to thermal conductivity, respectively (*1*).

During the past decades, great efforts have been devoted to enhancing thermoelectric materials' zT. Proven strategies are typified by enhancing power factor S^2/ρ through carrier concentration optimization (*2*) and band engineering (*3*) as well as by reducing lattice thermal conductivity through phonon scattering by defects (*4*), which have led to a notable improvement in various thermoelectrics including PbTe (*5*), Bi_2Te_3 (*6*, *7*), filled skutterudites (*8*), half-Heuslers (*9*), etc. Among known thermoelectrics for midtemperature (500 to 800 K) applications, GeTe-based materials stand out because of their high performance (*10*).

GeTe undergoes a continuous phase transition between a high-temperature cubic structure (c-GeTe) and a low-temperature rhombohedral structure (r-GeTe) at ~720 K because of the slight distortion along the [111] crystallographic direction (*11*). Such a symmetry breaking leads a notable difference in band structures between r-GeTe and c-GeTe (*12*, *13*). The band structure of c-GeTe is very similar to that of PbTe and SnTe, where the valence band maximum locates at L and the secondary valence band at Σ with a small energy offset (*13*). This leads early researches to mainly focus on c-GeTe (*14*, *15*), and indeed, a zT approaching 2 at ~800 K has been realized with decades of developments (*14*, *15*). Recently, r-GeTe has been revealed to show an even higher zT at ~600 K (*12*, *16*, *17*), enabled by the rearrangement of the symmetry reduction–induced split bands for a large band degeneracy (*12*, *18*). Moreover, this strategy can be manipulated to have a great effect on enhancing zT (of ~0.8) even at temperatures close to 300 K (*19*, *20*). These together indicate the high zT of GeTe in the entire midtemperature (500 to 800 K) for an efficient thermoelectric power generation.

The low formation energy of Ge vacancies helps understand the nature that pristine GeTe intrinsically comes with massive Ge vacancies, which result in a very high hole concentration (~10^{21} cm^{-3}) (*13*, *21*). A reduction of hole concentration to its optimum is essential for realizing the high zT of GeTe. Existing work usually use Bi (*13*, *22*) or Sb (*23*, *24*) as electron donors at Ge site, but this unfortunately leads to a decrease in carrier mobility (*23*, *24*). Recently, Cu_2Te is reported to be an extremely efficient agent for decreasing hole concentration with least detrimental effects on carrier mobility (*16*). A reduction of hole concentration from ~10^{21} to ~2×10^{20} cm^{-3} can be realized by only 1.5% Cu_2Te alloying (*16*). In addition, PbSe alloying was reported to be effective on reducing both hole concentration and lattice thermal conductivity (*25*). The underlying mechanism for reducing hole concentration in both cases is the suppression of Ge vacancies because of its largely increased formation energy upon alloying. This motivates the current work on a combination of both Cu_2Te and PbSe alloying for a simultaneous optimization of electron and phonon transport for an extraordinary performance.

One further step that has to be taken for realizing an efficient thermoelectric application of GeTe is the fabrication of high-efficiency devices. Both electrically and thermally conductive but chemically inert contacts between thermoelectric materials and electrodes are essential to ensure the high device efficiency offered by the high-performance materials (*26*, *27*). Usually, a stack of multiple layers can be applied for a prevention of atomic diffusion, a release of thermal expansion mismatch, and a reduction of contact resistance (*28*, *29*). For GeTe-based devices, Fe and Ni were considered as electrodes, yet a direct bond to GeTe results in a notable atomic diffusion thus a notable decrease in conduction and efficiency (*29*, *30*). Existing work indicates that alloys (*26*), compounds (*29*), and metals (*31*) can be used as a medium between thermoelectric materials and electrodes for inhibiting atomic diffusion.

In this work, an optimized carrier concentration of 1×10^{20} cm^{-3} was realized with 2% Cu_2Te + 10% PbSe alloying. Such a relatively low overall level of doping ensures the high carrier mobility at the

Interdisciplinary Materials Research Center, School of Materials Science and Engineering, Tongji University, 4800 Caoan Rd., Shanghai 201804, China.
*Corresponding author. Email: yanzhong@tongji.edu.cn

same time. In addition, PbSe alloying notably strengthens the scattering of phonons through mass and strain fluctuations. These together led to extraordinary thermoelectric zT over a broad temperature range. Using thermoelectric SnTe as a diffusion barrier, the Ag/SnTe/GeTe contact successfully enables a negligible extra resistance and a prevention of chemical diffusion, which results in a record single-leg device efficiency of ~14% under a ΔT ~ 440 K (cold side at 300 K).

RESULTS AND DISCUSSION

The details about material synthesis, characterizations, and property measurements (efficiency measurement setup in fig. S1) are given in the Supplementary Materials. A copper bar was used as a heat flow meter within a temperature difference of 0.5 to 2.5 K (table S1), which is determined by an average of 60 measurements with a relative SD of <3% (fig. S2) to ensure the large signal-to-noise ratio. A constant thermal conductivity of copper was used to estimate the heat flow, and less thermally conductive materials such as constantan (*32*, *33*) might be good choices as well for the heat flow meter. The powder x-ray diffraction (XRD) patterns (fig. S3) indicate a rhombohedral structure (*R*3*m*) of $[(GeTe)_{0.98}(Cu_2Te)_{0.02}]_{1-y}(PbSe)_y$ alloys for y up to 0.25 at room temperature. Scanning electron microscope (SEM) and energy-dispersive spectrometer (EDS) results confirm the formation of solid solutions.

Cu_2Te alloying enables a Hall carrier concentration (n_H) reduction while maintaining a high carrier mobility in GeTe (*16*) (Fig. 1, A and B), due to the negligible effect of Cu_2Te alloying on the crystal structure and thus the electronic structure of GeTe (*16*). A further increase in Cu_2Te alloying concentration of >2% does not lead to a further decrease in hole concentration according to our results, which can be understood by the limited solubility (*34*). Therefore, a fixed Cu_2Te alloying concentration of 2% is used for a further decrease in hole carrier concentration by a further PbSe alloying. The reduction in hole concentration can be understood by the increased formation energy of Ge vacancy through substituting with a larger cation (*25*). This is evidenced by the redissolution of Ge precipitates into the GeTe matrix (fig. S3). Two percent Cu_2Te and 25% PbSe coalloying enables a Hall carrier concentration to be as low as ~3×10^{19} cm^{-3}, successfully covering the optimal n_H of 6×10^{19} to 10×10^{19} cm^{-3} for GeTe thermoelectrics (depending on working temperatures) (*10*, *17*, *19*). An optimal n_H of 10×10^{19} cm^{-3} in this work only requires 2% Cu_2Te + 10% PbSe coalloying. Such a low n_H equivalently requires a sole PbSe alloying of more than 35% (*25*). The realization of an optimal n_H at a much lower concentration of alloy impurities (12% versus 35%) in this work ensures the high carrier mobility (Fig. 1B). Further, because of the increase in density-of-states effective mass (m^*) and thus an increase in Seebeck coefficient (Fig. 1C), which can be understood by the rearrangement of split valence bands induced by the crystallographic rhombohedral distorsion (*19*, *35*), a high power factor (S^2/ρ) is achieved (Fig. 1D).

The alloy defects induce strong fluctuations in both mass and strain, which notably strengthen the phonon scattering for a decrease in lattice thermal conductivity. The existence of alloying-induced lattice strains can be evidenced form the broadening in XRD peaks (*5*, *36*). As shown in the inset of Fig. 2B, where β is the "full width at half maximum (FWHM)" of the intense diffraction peaks and θ is the Bragg angle, the intercept of the linear fit between β and θ corresponds to the contribution of gain boundaries, while the slope stands for the contribution of substitutional defects. It can be seen that the materials in this work show a similar microstrain due to gain boundaries, but microstrain due to chemical substitution (slope) increases with increasing concentration of impurities. Furthermore, because of the resultant strong phonon scattering by alloy defects, lattice thermal conductivity (κ_L) can be as low as 0.6 W/m·K in alloys at 300 K (Fig. 2B). Here, κ_L is estimated by subtracting the electronic

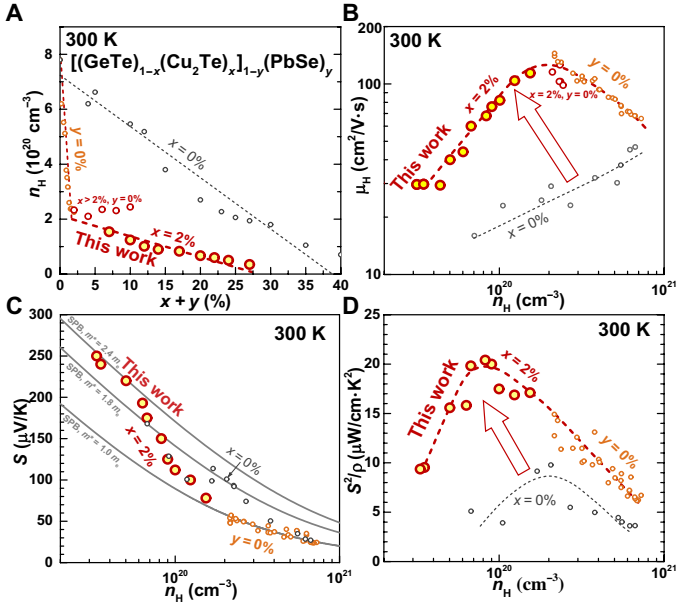

Fig. 1. Room temperature transport properties. Hall carrier concentration versus composition (**A**) and Hall carrier concentration–dependent Hall mobility (**B**), Seebeck coefficient (**C**), and power factor (**D**) for $(Ge_{1-x}Cu_{2x}Te)_{1-y}(PbSe)_y$ alloys at room temperature. Literature results are included for comparison (*16*, *25*). SPB, single parabolic band model.

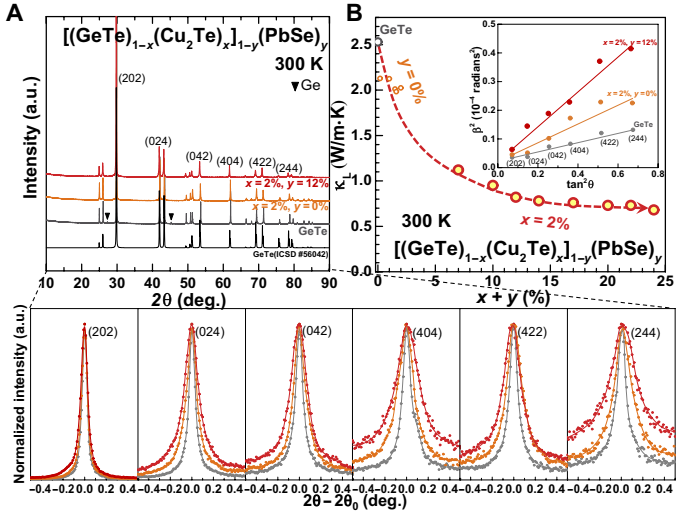

Fig. 2. Origin of low lattice thermal conductivity. Room temperature powder XRD patterns (*46*) (**A**), composition-dependent lattice thermal conductivity (*16*), and the lattice strain analyses for GeTe, $Ge_{0.98}Cu_{0.04}Te$, and $(Ge_{0.98}Cu_{0.04}Te)_{0.88}(PbSe)_{0.12}$ (**B**). a.u., arbitrary units; ICSD, inorganic crystal structure database.

component ($\kappa_E = LT/\rho$) from the total thermal conductivity (κ), where the Lorenz factor (L) is estimated by the single parabolic band approximation with acoustic phonon scattering (fig. S4A). Note that the slightly reduced sound velocity (fig. S4B) acts as another minor contributor to the κ_L reduction observed.

Detailed temperature-dependent thermoelectric properties for $(Ge_{0.98}Cu_{0.04}Te)_{1-y}(PbSe)_y$ alloys at 300 to 800 K are given in figs. S5 and S6. Because of the simultaneous optimization in carrier concentration with a high mobility and a reduction in lattice thermal conductivity, an extraordinary peak zT of >2.5 with an average $[zT_{avg} = (1/\Delta T)\int_{T_c}^{T_h} zT(T)\,dT]$ of 1.8 is realized within 300 to 800 K (Fig. 3). The high zT is further shown to be reproducible as confirmed by repeated measurements under a few thermal cycles (Fig. 3B and fig. S6). This enables this class of materials to be highly efficient for midtemperature waste-heat recovery (300 to 800 K). Note that the high zT can be realized in a broad composition range of $0.1 \le y \le 0.2$ (fig. S5D), which is an advantage for mass production. In addition, the compatibility factor is as high as ~6 V^{-1} and nearly temperature independent (fig. S7A), benefiting the realization of a high device efficiency (*37*).

The origin of peaking zT at particular temperatures is highly related to the band structure and phonon scattering. The phase transition from a high-temperature cubic structure to a low-temperature rhombohedral structure leads to a notable change in the valence band structure of GeTe (*35*, *38*, *39*), the rhombohedral angle of which ends up to be the critical indicator, and the overall valence band degeneracy maximizes in a rhombohedral structure but close to the cubic structure because of the rearrangement of the symmetry reduction–induced spilt bands (fig. S8A) (*13*, *38*). Such a rhombohedral angle depends on not only temperature but also composition (*12*). Previous studies (*16*) revealed that maintaining the pristine crystal structure with sufficient alloying ensures not only ensures a strong phonon scattering but also superior charge transport. In this work, Cu_2Te and PbSe coalloying induces negligible effect on the crystal structure (i.e., the rhombohedral angle; fig. S8B), leaving the temperature effect to dominate the band structure change. This enables the maximal valence band degeneracy to be realized in the temperature range interested (<750 K) for a high average performance.

To demonstrate the high thermoelectric efficiency enabled by the high-zT GeTe alloys, two single-leg thermoelectric devices are fabricated using $(Ge_{0.98}Cu_{0.04}Te)_{0.88}(PbSe)_{0.12}$ with a dimension of ~2 mm by 2 mm by 6.5 mm (Fig. 4A; details in the Supplementary Materials). In this work, Ag is found to bond with SnTe much stronger than that with GeTe. In addition, SnTe is confirmed to bond well with GeTe (*29*) with a negligible chemical diffusion. This enables a robust bonding without any cracks as confirmed by SEM observations taken before and after thermal cycling and long-term stability test (Fig. 4B and fig. S9). In addition, EDS mappings show clear boundaries of the heterostructures, suggesting SnTe as an effective diffusion barrier material.

Note that the SnTe diffusion barrier layer is only ~200 μm in thickness (~3% of the total length of the leg) and SnTe has a much higher thermal conductivity (8 W/m·K) as compared to that of GeTe alloys here (1 W/m·K) at room temperature (fig. S5C and fig. S10). Therefore, a large temperature gradient loss due to such a diffusion barrier is not expected. Moreover, SnTe has a good thermoelectric performance in p-type as well, which further guarantees a much larger thermoelectric output as compared to that of metal/alloy barriers, even if the temperature gradient loss in the barrier is large. SnTe is highly conductive, leading to a negligible (<2%) contribution of the hot-side diffusion barrier layer to the total inertial resistance of entire device even at a ΔT of 440 K. All these features make SnTe as a good choice as the diffusion barrier material here.

The total electrical contact resistance (including both electrode and diffusion barrier), measured by a four-probe technique (Fig. 4C), is found to be as low as ~0.2 milliohm. This corresponds to an interfacial contact resistivity (ρ_c) of only ~8 microhm·cm^2, which is one of the lowest among reported thermoelectric devices (fig. S11) (*26*, *29*, *31*). Note that the total resistance of contacts at both cold and hot sides is limited to be within 4% of the internal resistance (R_{in}) of the device, ensuring the high power output and conversion efficiency (*27*).

With a fixed cold side temperature of 300 K, the output voltage (V) as a function of current (I) under different temperature gradients (ΔT) is shown in Fig. 5A and fig. S12A. The nice linearity of V-I curves enables a determination of open-circuit voltage (V_{oc}) (the y intercept) and the internal resistance (R_{in}) (the slope), respectively. The

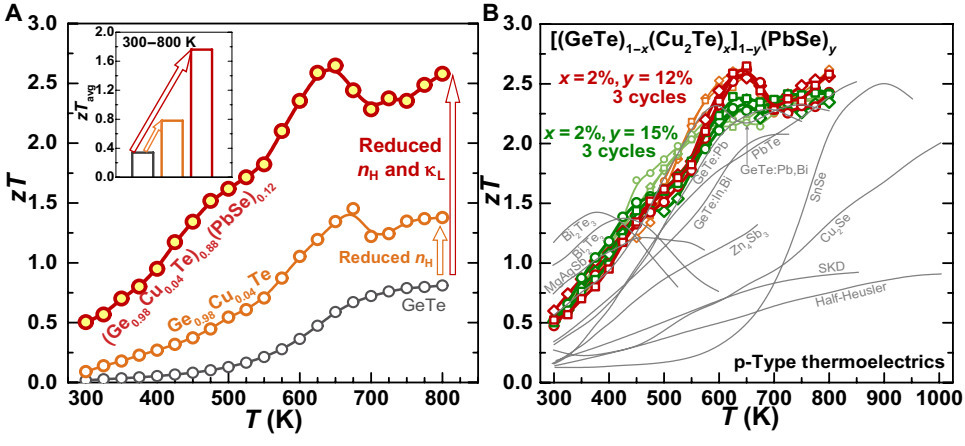

Fig. 3. Thermoelectric performance. Temperature-dependent figure of merit zT and the average zT within working temperatures (**A**) and the repeated measurements (**B**) for $(Ge_{0.98}Cu_{0.04}Te)_{1-y}(PbSe)_y$ alloys, with a comparison to that of known high-performance thermoelectrics (*5*, *7*, *8*, *12*, *14*, *28*, *43*, *47*–*51*). SKD, skutterudite.

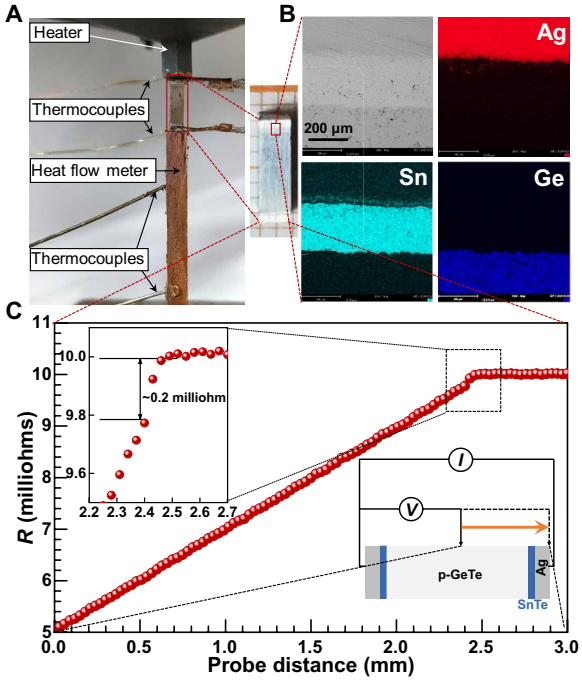

Fig. 4. Contact structures and resistance. (**A**) Experimental setup for the device efficiency measurement. Photo credit: Zhonglin Bu, Tongji University. (**B**) EDS mapping of the contacts. (**C**) Room temperature contact resistance using a line scanning technique.

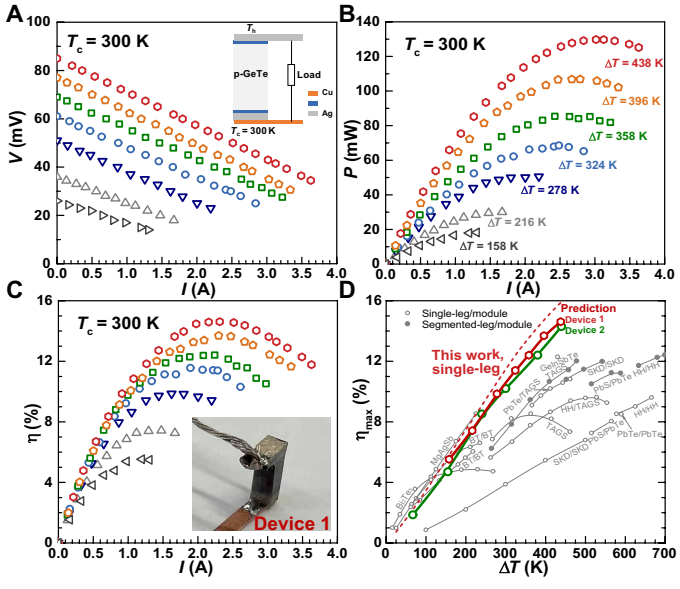

Fig. 5. Device properties. Current-dependent output voltage (**A**), output power (**B**), efficiency (**C**), and its maximum (**D**) for the single-leg devices under different temperature gradients, with a comparison to literature results (*6–9*, *28*, *40*, *41*, *43*, *52–54*) and prediction. TAGS, $(GeTe)_{1-x}(AgSbTe_2)_x$; HH, Half-Heusler; BT, Bi_2Te_3; SKD, skutterudite. Photo credit: Zhonglin Bu, Tongji University.

increase in V_{oc} and R_{in} with increasing ΔT (fig. S13) can be respectively understood by the increase in Seebeck coefficient and resistivity of GeTe alloys. Figure 5B and fig. S12B show the output power (P) at different ΔT, and the corresponding power density (per sectional area of thermoelectric material) is shown in fig. S14. The maximum output power is ~130 mW (corresponding to a power density of 25 kW/m^2) at $\Delta T \sim 440$ K, when the load resistance (R_{out}) is identical to the internal resistance (R_{in}). The measured device properties are reasonably consistent with predictions from the thermoelectric material (fig. S13).

Figure 5C and fig. S12C show the current-dependent efficiency (η) under different temperature gradients (ΔT). A measured maximum efficiency (η_{max}) is realized to be as high as ~14% at $\Delta T = 440$ K (Fig. 5D), which is actually higher than any of the experimental results in various devices reported before. Note that the η_{max} obtained in this work is highly comparable to that of conventional Bi_2Te_3 devices (*6*, *7*, *40*) and the recently reported MgAgSb one (*41*) near room temperature ($\Delta T < 250$ K), which can be understood by their comparable zT (fig. S7) as well as the stable and high compatibility factor of GeTe alloys at these temperatures. These together demonstrate the extraordinariness of GeTe thermoelectrics covering a broad temperature range.

Taking into account the contact resistance (assumed to be temperature independent) and compatibility factor (fig. S7), the predicted maximum efficiency from the temperature-dependent transport properties (*37*, *42*) is shown in Fig. 5D as a function of the applied temperature gradient. The measurement reasonably agrees with the prediction, suggesting a rational device design in this work for realizing nearly the full potential of GeTe alloy thermoelectrics for power generation. Note that the larger discrepancy at a higher temperature gradient can be understood by the larger heat loss at these high absolute temperatures (*9*, *43*).

Because of the phase transition between rhombohedral and cubic structure, one usually concerns the stability of GeTe-based devices. GeTe thermoelectrics are thermal-mechanically more robust than one would initially expect (*38*). This is firstly evidenced by the successful application of historical p-TAGS/n-PbTe devices (*40*, *44*). In addition, a recent work on GeTe devices was found to be stable for 450 thermal cycles (*31*). Furthermore, we demonstrate in two single-leg devices both a long-term stability (up to 200 hours) at $\Delta T = 400$ K (the hot-side temperature of 700 K, fig. S15) and a thermal cycle stability during heating/cooling (fig. S16). The good stability can be understood by the nature of a continuous phase transition [a smooth change in the rhombohedral angle (*12*, *45*)].

Note that the power measurement from the single-leg device excludes the heat exchange considerations because the hot- and cold-side temperatures are enforced with heaters and coolers and the temperatures are measured at the leg-exchanger interfaces. This is different from the measurement of a module because the heat exchangers would lead to temperature gradient losses. Therefore, additional efforts are needed in minimizing the thermal contact resistance of the heat exchangers to realize a module efficiency approaching the single-leg efficiency.

Summary

In summary, Cu_2Te and PbSe coalloying in GeTe simultaneously enables an optimization of hole concentration and a reduction in lattice thermal conductivity while maintaining a relatively high carrier mobility. This results in an outstanding figure of merit across a broad temperature range. The corresponding device efficiency of 14% is so far the highest for thermoelectric devices operating at a temperature gradient ΔT of <700 K. This work illustrates the extraordinariness

of GeTe thermoelectrics. The strategies developed here for both materials and devices might be applicable for other thermoelectrics.

MATERIALS AND METHODS

Synthesis

Polycrystalline GeTe, $Ge_{1-x}Cu_{2x}Te$, and $(Ge_{0.98}Cu_{0.04}Te)_{1-y}(PbSe)_y$ alloys were synthesized by melting, quenching, and annealing. The stoichiometric amounts of high-purity elements Ge (99.9999%), Te (99.999%), Cu (99.99%), Se (99.99%), and Pb (99.99%) were melted at 1223 K for 10 hours, followed by quenching in cold water and annealing at 850 K for 48 hours. The obtained ingots were ground into fine powder for XRD. Phase composition and microstructure are characterized by XRD (DX2000, PANalytical Aeris) and scanning electron microscope (Phenom Pro) equipped with an EDS. The dense (>95%) pellet samples with dimensions of ~12 mm in diameter and ~ 1.5 mm in thickness were obtained by hot-pressing at 823 K for 40 min under a uniaxial pressure of ~65 MPa.

Transport property measurements

The electrical properties including resistivity, Seebeck coefficient, and Hall coefficient were measured under helium. The Seebeck coefficient was obtained from the slope of thermopower versus temperature gradient within 0 to 5 K, where both the hot- and cold-side temperatures were measured by using two K-type thermocouples. The resistivity and Hall coefficient were measured by a four-probe Van Der Pauw technique under a reversible magnetic field of 1.5 T. The thermal conductivity (κ) is determined by $\kappa = dCpD$, where d, Cp, and D are density, heat capacity, and thermal diffusivity. The density was estimated by mass/volume, and the thermal diffusivity of GeTe-based alloys was measured by a laser flash technique (Netzsch LFA457). Both the electronic and thermal transport properties of GeTe-based alloys were performed in the temperature range of 300 to 800 K. The uncertainty in measurements of S, ρ, κ, and Hall coefficient is about 5%. Longitudinal (v_L) and transverse (v_T) sound velocities were measured on the pellet samples at room temperature, using an ultrasonic pulse receiver (Olympus NDT) equipped with an oscilloscope (Keysight).

SUPPLEMENTARY MATERIALS

Supplementary material for this article is available at http://advances.sciencemag.org/cgi/content/full/7/19/eabf2738/DC1

REFERENCES AND NOTES

1. A. F. Ioffe, *Semiconductor Thermoelements, and Thermoelectric Cooling* (Infosearch, 1957).
2. A. D. LaLonde, Y. Pei, G. J. Snyder, Reevaluation of $PbTe_{1-x}I_x$ as high performance n-type thermoelectric material. *Energ. Environ. Sci.* **4**, 2090–2096 (2011).
3. Y. Pei, X. Shi, A. LaLonde, H. Wang, L. Chen, G. J. Snyder, Convergence of electronic bands for high performance bulk thermoelectrics. *Nature* **473**, 66–69 (2011).
4. S. H. Li, J. M. Hinckley, J. Singh, P. K. Bhattacharya, Carrier velocity-field characteristics and alloy scattering potential in $Si_{1-x}Ge_x$/Si. *Appl. Phys. Lett.* **63**, 1393–1395 (1993).
5. Y. Wu, Z. Chen, P. Nan, F. Xiong, S. Lin, X. Zhang, Y. Chen, L. Chen, B. Ge, Y. Pei, Lattice strain advances thermoelectrics. *Joule* **3**, 1276–1288 (2019).
6. B. Zhu, X. Liu, Q. Wang, Y. Qiu, Z. Shu, Z. Guo, Y. Tong, J. Cui, M. Gu, J. He, Realizing record high performance in n-type Bi_2Te_3-based thermoelectric materials. *Energ. Environ. Sci.* **13**, 2106–2114 (2020).
7. F. Hao, P. Qiu, Y. Tang, S. Bai, T. Xing, H.-S. Chu, Q. Zhang, P. Lu, T. Zhang, D. Ren, J. Chen, X. Shi, L. Chen, High efficiency Bi_2Te_3-based materials and devices for thermoelectric power generation between 100 and 300 °C. *Energ. Environ. Sci.* **9**, 3120–3127 (2016).
8. Q. Zhang, J. Liao, Y. Tang, M. Gu, C. Ming, P. Qiu, S. Bai, X. Shi, C. Uher, L. Chen, Realizing a thermoelectric conversion efficiency of 12% in bismuth telluride/skutterudite segmented modules through full-parameter optimization and energy-loss minimized integration. *Energ. Environ. Sci.* **10**, 956–963 (2017).
9. J. Yu, Y. Xing, C. Hu, Z. Huang, Q. Qiu, C. Wang, K. Xia, Z. Wang, S. Bai, X. Zhao, L. Chen, T. Zhu, Half-Heusler thermoelectric module with high conversion efficiency and high power density. *Adv. Energy Mater.* **10**, 2000888 (2020).
10. D. Wu, L. Xie, X. Xu, J. He, High thermoelectric performance achieved in GeTe–Bi_2Te_3 Pseudo-binary via van der Waals gap-induced hierarchical ferroelectric domain structure. *Adv. Funct. Mater.* **29**, 1806613 (2019).
11. T. Rosenthal, M. N. Schneider, C. Stiewe, M. Döblinger, O. Oeckler, Real structure and thermoelectric properties of GeTe-rich germanium antimony tellurides. *Chem. Mater.* **23**, 4349–4356 (2011).
12. J. Li, X. Zhang, Z. Chen, S. Lin, W. Li, J. Shen, I. T. Witting, A. Faghaninia, Y. Chen, A. Jain, L. Chen, G. J. Snyder, Y. Pei, Low-symmetry rhombohedral GeTe thermoelectrics. *Joule* **2**, 976–987 (2018).
13. J. Li, Z. Chen, X. Zhang, Y. Sun, J. Yang, Y. Pei, Electronic origin of the high thermoelectric performance of GeTe among the p-type group IV monotellurides. *NPG Asia Mater.* **9**, e353 (2017).
14. Y. Gelbstein, J. Davidow, S. N. Girard, D. Y. Chung, M. Kanatzidis, Controlling metallurgical phase separation reactions of the $Ge_{0.87}Pb_{0.13}Te$ alloy for high thermoelectric performance. *Adv. Energy Mater.* **3**, 815–820 (2013).
15. M. Li, M. Hong, X. Tang, Q. Sun, W.-Y. Lyu, S.-D. Xu, L.-Z. Kou, M. Dargusch, J. Zou, Z.-G. Chen, Crystal symmetry induced structure and bonding manipulation boosting thermoelectric performance of GeTe. *Nano Energy* **73**, 104740 (2020).
16. Z. Bu, W. Li, J. Li, X. Zhang, J. Mao, Y. Chen, Y. Pei, Dilute Cu_2Te-alloying enables extraordinary performance of r-GeTe thermoelectrics. *Mater. Today Phys.* **9**, 100096 (2019).
17. J. Dong, F.-H. Sun, H. Tang, J. Pei, H.-L. Zhuang, H.-H. Hu, B.-P. Zhang, Y. Pan, J.-F. Li, Medium-temperature thermoelectric GeTe: Vacancy suppression and band structure engineering leading to high performance. *Energ. Environ. Sci.* **12**, 1396–1403 (2019).
18. J. E. Lewis, Band sturcture and nature of lattice defect in GeTe from analysis of electrical properties. *Phys. Stat. Sol.* **35**, 737–745 (1969).
19. Z. Bu, Z. Chen, X. Zhang, S. Lin, J. Mao, W. Li, Y. Chen, Y. Pei, Near-room-temperature rhombohedral $Ge_{1-x}Pb_xTe$ thermoelectrics. *Mater. Today Phys.* **15**, 100260 (2020).
20. L. Wang, J. Li, C. Zhang, T. Ding, Y. Xie, Y. Li, F. Liu, W. Ao, C. Zhang, Discovery of low-temperature GeTe-based thermoelectric alloys with high performance competing with Bi_2Te_3. *J. Mater. Chem. A* **8**, 1660–1667 (2020).
21. D. H. Damon, M. S. Lubell, R. Mazelsky, Nature of the defects in germanium telluride. *J. Phys. Chem. Solids* **28**, 520–522 (1967).
22. S. Perumal, S. Roychowdhury, K. Biswas, Reduction of thermal conductivity through nanostructuring enhances the thermoelectric figure of merit in $Ge_{1-x}Bi_xTe$. *Inorg Chem Front* **3**, 125–132 (2016).
23. J. Li, X. Zhang, S. Lin, Z. Chen, Y. Pei, Realizing the high thermoelectric performance of GeTe by Sb-doping and Se-alloying. *Chem. Mater.* **29**, 605–611 (2017).
24. M. Hong, Y. Wang, T. Feng, Q. Sun, S. Xu, S. Matsumura, S. T. Pantelides, J. Zou, Z. G. Chen, Strong phonon–phonon interactions securing extraordinary thermoelectric $Ge_{1-x}Sb_xTe$ with Zn-alloying-induced band alignment. *J. Am. Chem. Soc.* **141**, 1742–1748 (2019).
25. J. Li, Z. Chen, X. Zhang, H. Yu, Z. Wu, H. Xie, Y. Chen, Y. Pei, Simultaneous optimization of carrier concentration and alloy scattering for ultrahigh performance GeTe thermoelectrics. *Adv. Sci. (Weinh)* **4**, 1700341 (2017).
26. J. Li, S. Zhao, J. Chen, C. Han, L. Hu, F. Liu, W. Ao, Y. Li, H. Xie, C. Zhang, Al-Si alloy as a diffusion barrier for GeTe-based thermoelectric legs with high interfacial reliability and mechanical strength. *ACS Appl. Mater. Interfaces* **12**, 18562–18569 (2020).
27. W. Liu, Q. Jie, H. S. Kim, Z. Ren, Current progress and future challenges in thermoelectric power generation: From materials to devices. *Acta Mater.* **87**, 357–376 (2015).
28. S. Perumal, M. Samanta, T. Ghosh, U. S. Shenoy, A. K. Bohra, S. Bhattacharya, A. Singh, U. V. Waghmare, K. Biswas, Realization of high thermoelectric figure of merit in GeTe by complementary Co-doping of Bi and In. *Joule* **3**, 2565–2580 (2019).
29. A. Singh, S. Bhattacharya, C. Thinaharan, D. K. Aswal, S. K. Gupta, J. V. Yakhmi, K. Bhanumurthy, Development of low resistance electrical contacts for thermoelectric devices based on n-type PbTe and p-type TAGS-85 $((AgSbTe_2)_{0.15}(GeTe)_{0.85})$. *J. Phys. D Appl. Phys.* **42**, 015502 (2009).
30. R. He, G. Schierning, K. Nielsch, Thermoelectric devices: A review of devices, architectures, and contact optimization. *Adv. Mater. Technol.* **3**, 1700256 (2018).
31. T. Xing, Q. Song, P. Qiu, Q. Zhang, X. Xia, J. Liao, R. Liu, H. Huang, J. Yang, S. Bai, D. Ren, X. Shi, L. Chen, Superior performance and high service stability for GeTe-based thermoelectric compounds. *Natl. Sci. Rev.* **6**, 944–954 (2019).
32. Q. Zhu, S. Song, H. Zhu, Z. Ren, Realizing high conversion efficiency of Mg_3Sb_2-based thermoelectric materials. *J. Power Sources* **414**, 393–400 (2019).
33. J. Jiang, H. Zhu, Y. Niu, Q. Zhu, S. Song, T. Zhou, C. Wang, Z. Ren, Achieving high room-temperature thermoelectric performance in cubic AgCuTe. *J. Mater. Chem. A* **8**, 4790–4799 (2020).

34. O. S. Gogishvili, I. P. Lavrinenko, S. P. Lalykhin, Behavior of copper in germanium telluride. *Inorganic Materials (translated from Neorganicheskie Materialy)* **10**, 307–311 (1982).
35. J. Shuai, X. J. Tan, Q. Guo, J. T. Xu, A. Gellé, R. Gautier, J. F. Halet, F. Failamani, J. Jiang, T. Mori, Enhanced thermoelectric performance through crystal field engineering in transition metal–doped GeTe. *Mater. Today Phys.* **9**, 100094 (2019).
36. J. J. Urban, Anharmonic convergence: Tuning two dials on phonons for high zT in p-type PbTe. *Joule* **3**, 1180–1181 (2019).
37. G. J. Snyder, T. S. Ursell, Thermoelectric efficiency and compatibility. *Phys. Rev. Lett.* **91**, 148301 (2003).
38. X. Zhang, Z. Bu, S. Lin, Z. Chen, W. Li, Y. Pei, GeTe Thermoelectrics. *Joule* **5**, 986–1003 (2020).
39. Z. Liu, W. Gao, W. Zhang, N. Sato, Q. Guo, T. Mori, High power factor and enhanced thermoelectric performance in Sc and Bi codoped GeTe: Insights into the hidden role of rhombohedral distortion degree. *Adv. Energy Mater.* **10**, 2002588 (2020).
40. A. K. Bohra, R. Bhatt, A. Singh, S. Bhattacharya, R. Basu, K. N. Meshram, S. K. Sarkar, P. Bhatt, P. K. Patro, D. K. Aswal, K. P. Muthe, S. C. Gadkari, Transition from n- to p-type conduction concomitant with enhancement of figure-of-merit in Pb doped bismuth telluride: Material to device development. *Mater. Design* **159**, 127–137 (2018).
41. D. Kraemer, J. Sui, K. McEnaney, H. Zhao, Q. Jie, Z. F. Ren, G. Chen, High thermoelectric conversion efficiency of MgAgSb-based material with hot-pressed contacts. *Energ. Environ. Sci.* **8**, 1299–1308 (2015).
42. G. J. Snyder, A. H. Snyder, Figure of merit *ZT* of a thermoelectric device defined from materials properties. *Energ. Environ. Sci.* **10**, 2280–2283 (2017).
43. Y. Xing, R. Liu, J. Liao, Q. Zhang, X. Xia, C. Wang, H. Huang, J. Chu, M. Gu, T. Zhu, C. Zhu, F. Xu, D. Yao, Y. Zeng, S. Bai, C. Uher, L. Chen, High-efficiency half-Heusler thermoelectric modules enabled by self-propagating synthesis and topologic structure optimization. *Energ. Environ. Sci.* **12**, 3390–3399 (2019).
44. P. Thomas, B. Cook, D. Stokes, G. Krueger, R. Venkatasubramanian, Scalable thermoelectric (TE) device technologies for power generation. *Proc. Spin* **8377**, 83770H (2012).
45. B. A. Cook, M. J. Kramer, X. Wei, J. L. Harringa, E. M. Levin, Nature of the cubic to rhombohedral structural transformation in $(AgSbTe_2)_{15}(GeTe)_{85}$ thermoelectric material. *J. Appl. Phys.* **101**, 053715 (2007).
46. H. Wiedemeier, P. A. Siemers, The thermal expansion of GeS and GeTe. *Z. Anorg. Allg. Chem.* **431**, 299–304 (1977).
47. B. Poudel, Q. Hao, Y. Ma, Y. Lan, A. Minnich, B. Yu, X. Yan, D. Wang, A. Muto, D. Vashaee, X. Chen, J. Liu, M. S. Dresselhaus, G. Chen, Z. Ren, High-thermoelectric performance of nanostructured bismuth antimony telluride bulk alloys. *Science* **320**, 634–638 (2008).
48. G. Snyder, M. Christensen, E. Nishibori, T. Caillat, B. Iversen, Disordered zinc in Zn_4Sb_3 with phonon-glass and electron-crystal thermoelectric properties. *Nat. Mater.* **3**, 458–463 (2004).
49. L. D. Zhao, S. H. Lo, Y. Zhang, H. Sun, G. Tan, C. Uher, C. Wolverton, V. P. Dravid, M. G. Kanatzidis, Ultralow thermal conductivity and high thermoelectric figure of merit in SnSe crystals. *Nature* **508**, 373–377 (2014).
50. P. Qiu, T. Mao, Z. Huang, X. Xia, J. Liao, M. T. Agne, M. Gu, Q. Zhang, D. Ren, S. Bai, X. Shi, G. J. Snyder, L. Chen, High-efficiency and stable thermoelectric module based on liquid-like materials. *Joule* **3**, 1538–1548 (2019).
51. H. Zhao, J. Sui, Z. Tang, Y. Lan, Q. Jie, D. Kraemer, K. McEnaney, A. Guloy, G. Chen, Z. Ren, High thermoelectric performance of MgAgSb-based materials. *Nano Energy* **7**, 97–103 (2014).
52. B. Jiang, X. Liu, Q. Wang, J. Cui, B. Jia, Y. Zhu, J. Feng, Y. Qiu, M. Gu, Z. Ge, J. He, Realizing high-efficiency power generation in low-cost PbS-based thermoelectric materials. *Energ. Environ. Sci.* **13**, 579–591 (2020).
53. P. Jood, M. Ohta, A. Yamamoto, M. G. Kanatzidis, Excessively doped PbTe with Ge-induced nanostructures enables high-efficiency thermoelectric modules. *Joule* **2**, 1339–1355 (2018).
54. L. I. Anatychuk, L. N. Vikhor, L. T. Strutynska, I. S. Termena, Segmented generator modules using Bi_2Te_3-based materials. *J. Electron Mater.* **40**, 957–961 (2011).
55. W. Li, L. Zheng, B. Ge, S. Lin, X. Zhang, Z. Chen, Y. Chang, Y. Pei, Promoting SnTe as an eco-friendly solution for p-PbTe thermoelectric via band convergence and interstitial defects. *Adv. Mater.* **29**, 1605887 (2017).
56. M. Gu, X. Xia, X. Huang, S. Bai, X. Li, L. Chen, Study on the interfacial stability of p-type $Ti/Ce_yFe_xCo4_{-x}Sb_{12}$ thermoelectric joints at high temperature. *J. Alloy Compd.* **671**, 238–244 (2016).
57. G. J. Snyder, Thermoelectric power generation: Efficiency and compatibility, in *Thermoelectric Handbook: Macro to Nano*, D. M. Rowe, Ed. (CRC Taylor & Francis Group, 2006) vol. 9, pp. 1–26.
58. J. Li, W. Li, Z. Bu, X. Wang, B. Gao, F. Xiong, Y. Chen, Y. Pei, Thermoelectric transport properties of $Cd_xBi_yGe_{1-x-y}Te$ Alloys. *ACS Appl. Mater. Interfaces* **10**, 39904–39911 (2018).
59. M. Gu, X. Xia, X. Li, X. Huang, L. Chen, Microstructural evolution of the interfacial layer in the $Ti–Al/Yb_{0.6}Co_4Sb_{12}$ thermoelectric joints at high temperature. *J. Alloy Compd.* **610**, 665–670 (2014).
60. X. Y. Yang, J. H. Wu, M. Gu, X. G. Xia, L. D. Chen, Fabrication and contact resistivity of $W–Si_3N_4/TiB_2–Si_3N_4$/p–SiGe thermoelectric joints. *Ceram. Int.* **42**, 8044–8050 (2016).
61. P. H. Ngan, N. Van Nong, L. T. Hung, B. Balke, L. Han, E. M. J. Hedegaard, S. Linderoth, N. Pryds, On the challenges of reducing contact resistances in thermoelectric generators based on half-Heusler alloys. *J. Electron. Mater.* **45**, 594–601 (2015).
62. J. García-Cañadas, G. Min, Preparation and characterisation of contacts for high temperature thermoelectric modules. *AIP Conf/ Proc.* **1449**, 454–457 (2012).

Acknowledgments: We thank J. Luo from Shanghai University for the support on the XRD measurements. **Funding:** This work was financially supported by the National Natural Science Foundation of China (grant nos. 51861145305 and 51772215), the National Key Research and Development Program of China (2018YFB0703600), the Innovation Program of Shanghai Municipal Education Commission, and China National Postdoctoral Program for Innovative Talents (BX20200237). **Author contributions:** Y.P. conceptualized this work. Z.B., B.S., and J.T. carried out the experiments. Z.B., Z.C., and S.L. collected the literature data. Z.B., X.Z., W.L., and Y.P. wrote the manuscript. All authors discussed the results and provided feedback on the manuscript. **Competing interests:** The authors declare that they have no competing interests. **Data and materials availability:** All data needed to evaluate the conclusions in the paper are present in the paper and/or the Supplementary Materials.

Submitted 15 October 2020
Accepted 19 March 2021
Published 7 May 2021
10.1126/sciadv.abf2738

Citation: Z. Bu, X. Zhang, B. Shan, J. Tang, H. Liu, Z. Chen, S. Lin, W. Li, Y. Pei, Realizing a 14% single-leg thermoelectric efficiency in GeTe alloys. *Sci. Adv.* **7**, eabf2738 (2021).

Realizing a 14% single-leg thermoelectric efficiency in GeTe alloys

Zhonglin Bu, Xinyue Zhang, Bing Shan, Jing Tang, Hongxia Liu, Zhiwei Chen, Siqi Lin, Wen Li and Yanzhong Pei

Sci Adv **7** (19), eabf2738.
DOI: 10.1126/sciadv.abf2738